Structural and morphological study of mechanochemically synthesized crystalline nanoneedles of Zr-doped carbonated chlorapatite

Bahman Nasiri-Tabrizi [a,b], Erfan Zalnezhad [c,*], Belinda Pingguan-Murphy [a,**], Wan Jefrey Basirun [d], A.M.S. Hamouda [e], Saeid Baradaran [b]

[a] Department of Biomedical Engineering, Faculty of Engineering, University of Malaya, 50603 Kuala Lumpur, Malaysia
[b] Department of Mechanical Engineering, Faculty of Engineering, University of Malaya, 50603 Kuala Lumpur, Malaysia
[c] Department of Mechanical Engineering, Hanyang University, 222 Wangsimni-ro, Seongdong-gu, Seoul, 133-791, Korea
[d] Department of Chemistry, Faculty of Science, University of Malaya, 50603 Kuala Lumpur, Malaysia
[e] Mechanical and Industrial Engineering Department, College of Engineering, Qatar University, P.O. Box 2713, Doha, Qatar

ARTICLE INFO

Article history:
Received 9 October 2014
Accepted 25 February 2015
Available online 5 March 2015

Keywords:
Biomaterials
Powder technology
Phase transformation
Nanoneedles

ABSTRACT

Nanosize Zr-doped carbonated chlorapatite (n-ZCCA) was developed as a novel bioceramic by a ball milling process. Results showed that the microstructural characteristics of the product were affected significantly by the degree of substitution and subsequent annealing at 800 °C for 1 h. In the absence of zirconium, mechanical activation for 3 h resulted in the formation of carbonated hydroxyapatite (CHA). With the addition of various amounts of zirconium, nanosize Zr-doped carbonated chlorhydroxyapatite (n-ZCCHA) and n-ZCCA were formed as a result of progressive mechanochemical reactions. From the HR-TEM images, the preferential substitution of Zr onto the *ac* or *bc* chlorapatite crystal facets (rich in calcium ions) led to a *c*-axis oriented crystal growth of crystalline nanoneedles with an average size of around 40–60 nm in length and 10–20 nm in width.

1. Introduction

Bioceramics are an important subset of biomaterials with wide range in biocompatibility, from the ceramic oxides to the other extreme of resorbable materials [1]. There have been significant advances in this field in hard-tissue replacement and regeneration over the last decade or so [2]. Recently, it has been found that doping or modification of original hexagonal apatite crystal structure with various ions such as Ca^{2+}, Mg^{2+}, Sr^{2+}, Ba^{2+}, Mn^{2+}, Fe^{2+}, Zn^{2+}, Cd^{2+}, Pb^{2+}, Na^{+}, K^{+}, Al^{3+}, PO_4^{3-}, AsO_4^{3-}, VO_4^{3-}, SO_4^{3-}, CO_3^{2-}, SiO_4^{3-}, OH^{-}, F^{-}, Cl^{-}, Br^{-}, and O^{2-} can improve the phase stability, mechanical and electrical properties as well as biological responses [3,4]. Therefore, current biomedical applications of these modified bioceramics may include substitutions for hips, knees, teeth, tendons and ligaments, as well as restoration for periodontal disease, maxillofacial reconstruction, augmentation and stabilization of the jawbone, spinal fusion and bone fillers after tumor surgery [5]. Besides, these bioceramics have potential applications in drug-delivery systems [6] and tissue engineering applications [7].

The substitution of Zr ions in different ceramic lattices have shown improvements in optical transparency [8], mechanical flexibility [9], critical current density and upper critical field [10] as well as an increment of photocatalytic degradation of bisphenol A (BPA) [11]. In the field of bioceramics, this replacement can improve the mechanical properties and biological responses [12]. To the best of our knowledge, the role of Zr substitution in the apatite crystal growth orientation, however, remains unaddressed. Hence, in the present study, the structural and morphological features of mechanochemically synthesized n-ZCCA are explored for the first time.

2. Materials and methods

$Ca(OH)_2$ ($\geq$96 wt%), H_3PO_4 ($\geq$85 wt% in H_2O), and $ZrCl_4$ (99.99 wt%) (all from Sigma-Aldrich Co., USA) were used as reactants. The designed level of replacement of Ca by Zr is shown by the *x* value in the CA, where the *x* values are 0.0, 0.25, 0.50, and 1.0 and consequently the products were labeled as Z0, Z0.25, Z0.5 and Z1, respectively (see Supplementary data 1). Adequate amounts of reagents were first blended and the mixed powders were milled for 3 h in a high-energy planetary ball mill (Retsch, PM100) using zirconia vials and balls (see Supplementary data 2). The general form of the reaction is as follows (see Eq. (1) and Supplementary data 2). To study the influence of subsequent

* Corresponding author. Tel.: +82 2 2220 0431; fax: +82 2 2292 3406.
** Corresponding author. Tel.: +603 79674491; fax: +603 79674579.
E-mail addresses: erfan_zalnezhad@yahoo.com (E. Zalnezhad), bpingguan@um.edu.my (B. Pingguan-Murphy).

http://dx.doi.org/10.1016/j.matlet.2015.02.125
0167-577X/

annealing on the structural evolutions, the milled specimens were annealed under atmospheric pressure at 800 °C for 1 h.

$$(10-x-y)Ca(OH)_2+(6-y)H_3PO_4+xZrCl_4+yH_2CO_3 \text{ (from air)} \rightarrow Ca_{10-x-y}Zr_x(PO_4)_{6-y}(CO_3)_y(OH)_{2-y-2x}Cl_{2x}+xCl_2+(18-y)H_2O \quad (1)$$

The phase compositions were checked by powder X-ray diffraction (XRD) analysis with a PANalytical Empyrean X-ray diffractometer (Cu-K_α radiation) over a 2θ range from 10° to 70°. To identify the functional groups of nanopowders, attenuated total reflection (ATR) analysis was carried out on a Tensor 27 (Bruker FT-

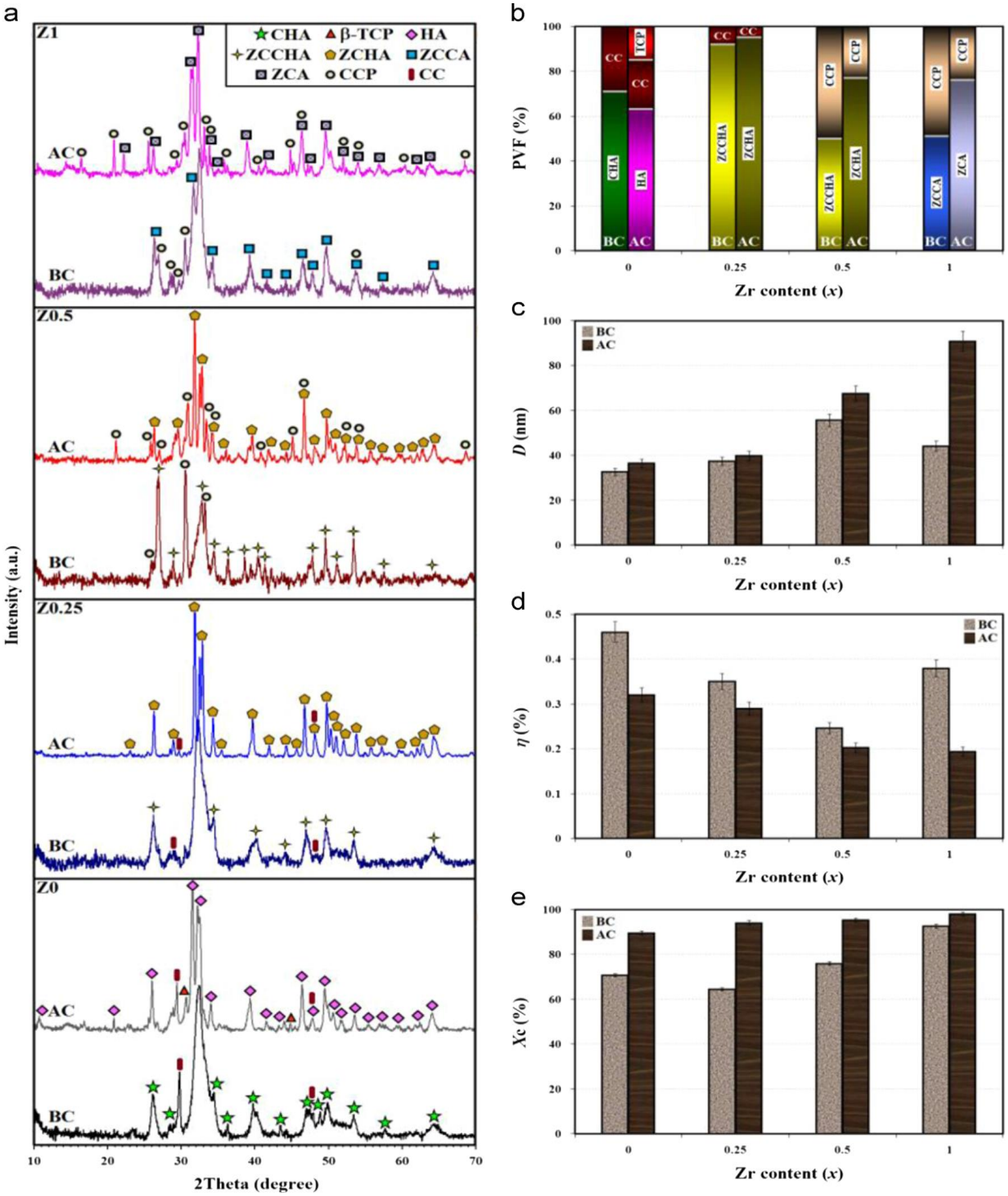

Fig. 1. (a) XRD profiles, (b) phase volume fraction (PVF, %), (c) crystallite size (D, nm), (d) lattice strain (η, %), and (e) crystallinity degrees (Xc, %) of the 3 h milled specimens before and after annealing at 800 °C for 1 h.

IR spectrophotometer) with a frequency range of 4000–400 cm^{-1}. The microstructure of the products was analyzed using FE-SEM/EDS (SU8000, Hitachi, Japan) and TEM (HT-7700, Hitachi, Japan).

3. Results and discussion

Fig. 1a shows the XRD profiles of 3 h milled specimens before and after annealing. In the absence of Zr, milling for 3 h resulted in the formation of CHA ($Ca_{10-y}(PO_4)_{6-y}(CO_3)_y(OH)_{2-y}$, JCPDS019-0272). With the x value of 0.25 (Z0.25), ZCCHA ($Ca_{9.75-y}Zr_{0.25}(PO_4)_{6-y}(CO_3)_y(OH)_{1.5-y}Cl_{0.5}$) was formed with the same milling time. In addition, calcium carbonate ($CaCO_3$, JCPDS01-072-1651) appeared as a secondary phase in the XRD profile. With the increase of Zr concentration in Z0.5, the intensity of the characteristic peaks of ZCCHA declined notably and new diffraction peaks attributed to calcium chlorophosphate (CCP, Ca_2PO_4Cl, JCPDS01-072-0010) emerged due to the incomplete reaction of the raw materials. Further increasing the Zr content to $x=1$ (Z1) led to the formation of ZCCA ($Ca_{9-y}Zr_y(PO_4)_{6-y}(CO_3)_yCl_2$, JCPDS027-0074) due to the gradual mechanochemical reactions. The transition from CHA to hydroxyapatite (HA, JCPDS01-070-0798) and tricalcium phosphate (β-TCP, JCPDS09-0169) was observed in the heat treated Z0, where the volume fractions of HA and β-TCP were 80 ± 4 and $20 \pm 1\%$, respectively (Fig. 1b). This phase decomposition is related to the temperature which the HA transformation take place, from a poorly crystalline apatite to a highly crystalline structure [13]. In a similar trend, the highly crystalline Zr-doped chlorhydroxyapatite (ZCHA, $Ca_{10-x}Zr_x(PO_4)_6(OH)_{2-2x}Cl_{2x}$, JCPDS01-070-0798) was formed after annealing of Z0.25 and Z0.5. After annealing of Z1, ZCCA crystallized to Zr-doped chlorapatite (ZCA, $Ca_{10-y}Zr_y(PO_4)_6Cl_2$) and consequently the phase compositions were ZCA and CCP. Before thermal treatment, the values of a-axis, c-axis, and unit cell volume of the apatite lattice were 9.55583 Å, 6.76548 Å and 535.02 $Å^3$, respectively. The incorporation of Zr into the apatite structure resulted in the shrinkage of the lattice constants, as the radius of Zr^{4+} (0.82 Å) is smaller compared to Ca^{2+} (1.00 Å) [14]. After annealing, due to the recovery of the crystal lattice, the unit cell volume increased to 543.40 $Å^3$.

From Fig. 1c–e, the structural features of the products are influenced significantly by the level of a substitution and subsequent annealing process. Here, crystallite size (D) and lattice strain (η) of the samples were calculated using the XRD data [15]. In Fig. 1c, there is a positive linear correlation between Zr content and crystallite size until $x=0.5$. From this value on, the correlation is negative. It seems that the addition of Zr up to $x=0.50$ can promote surface diffusion, densification and grain growth which resulted in an increase in the crystallite size [16]. As the Zr concentration increased further to $x=1.0$, the crystallite size decreased to 44 ± 2 nm and lattice strain increased to $0.37 \pm 0.02\%$. These opposite changes suggest that Zr content equal to $x=1.0$ effectively inhibits grain growth probably by staying at grain boundaries which leads to a reduction in the crystallite size and an enhancement in lattice strain. After annealing, an apparent increase in the crystallite size (90 ± 4 nm) and a significant reduction in the lattice strain ($0.19 \pm 0.01\%$) was perceived, which are probably due to the completion of crystal recovery and further reduction in the internal energy (achieved by reducing the total area of grain boundary) [17]. Moreover, the crystallinity degree (Xc) was determined by taking the sum total of relative intensities of individual characteristic peaks [18]. Results show that the crystallinity degree of the heat treated Z0 is $89 \pm 2\%$ but increased to $97 \pm 2\%$ in the annealed Z1 (see Supplementary data 3).

The ATR spectra of the 3 h milled samples are shown in Fig. 2. The low intensity OH-derived band at 638 cm^{-1}, the disappearance of OH stretching band at 3573 cm^{-1} and the broadening of PO_4-derived bands are due to the decrease of crystallinity from the carbonate substitution in the apatite lattice [19]. With the presence of Zr, the

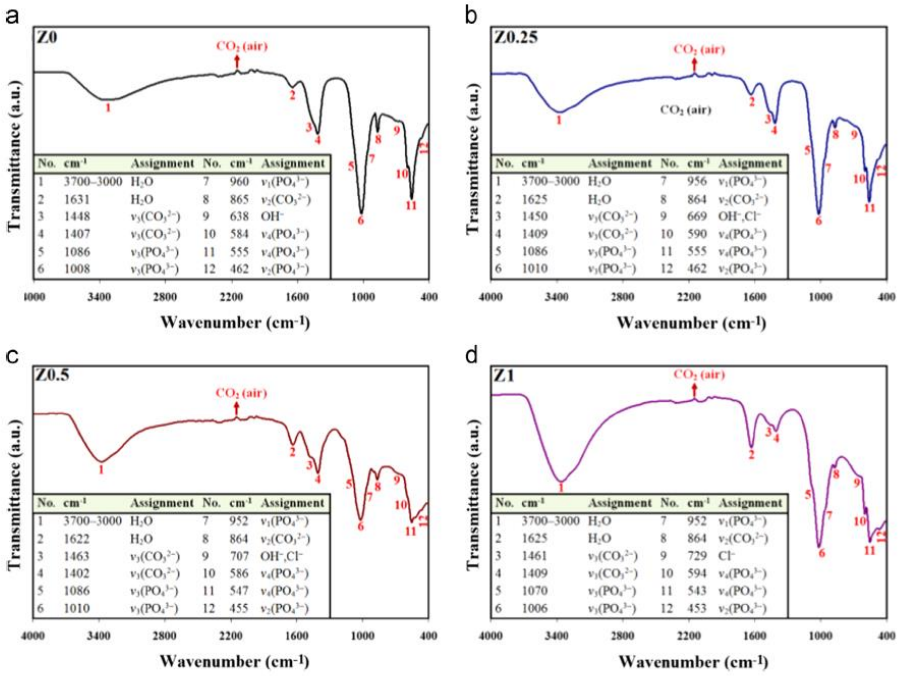

Fig. 2. ATR spectra of the milled samples with different degrees of substitution (a) Z0, (b) Z0.25, (c) Z0.5, and (d) Z1.

http://ac.els-cdn.com/S0167577X15003432/1-s2.0-S0167577X15003432-main.pdf?_tid=3434a7a4-4010-11e5-b09d-00000aab0f01&acdnat=1439287584_67007c8fa2ccc849d8e7a485eb3af1fa